
Stochastic Normalizing Flows

Hao Wu¹ Jonas Köhler² Frank Noé^{2,3,4}

Abstract

Normalizing flows are popular generative learning methods that train an invertible function to transform a simple prior distribution into a complicated target distribution. Here we generalize the framework by introducing Stochastic Normalizing Flows (SNF) – an arbitrary sequence of deterministic invertible functions and stochastic processes such as Markov Chain Monte Carlo (MCMC) or Langevin Dynamics. This combination can be powerful as adding stochasticity to a flow helps overcoming expressiveness limitations of a chosen deterministic invertible function, while the trainable flow transformations can improve the sampling efficiency over pure MCMC. Key to our approach is that we can match a marginal target density without having to marginalize out the stochasticity of traversed paths. Invoking ideas from nonequilibrium statistical mechanics, we introduce a training method that only uses conditional path probabilities. We can turn an SNF into a Boltzmann Generator that samples asymptotically unbiased from a given target density by importance sampling of these paths. We illustrate the representational power, sampling efficiency and asymptotic correctness of SNFs on several benchmarks.

1. Introduction

Normalizing flows (NF) are popular generative learning methods (Tabak et al., 2010; Tabak & Turner, 2013; Dinh et al., 2014; Rezende & Mohamed, 2015). Learned is an invertible function that transforms an easy-to-sample prior distribution into the desired target distribution. Due to the invertibility, the exact probability density of a sample generated by the flow can be computed. This allows us to train generative models by minimizing the Kullback-Leibler (KL) divergence to the target or by maximizing the likelihood (ML) of the observations without invoking a variational bound. Moreover, having access to tractable density is useful in variational inference (Rezende & Mohamed, 2015; Tomczak & Welling, 2016; Louizos & Welling, 2017; Berg et al., 2018) or approximate sampling

from distributions given by an energy function (Oord et al., 2017). A common problem in physics applications is the generation of asymptotically unbiased samples from energy models, i.e., target distribution defined up to a normalization constant. This can be achieved by combining flows with importance sampling methods to Boltzmann Generators (Noé et al., 2019), an approach now popular in molecular and material sciences and nuclear physics (Müller et al., 2018; Li & Wang, 2018; Noé et al., 2019; Köhler et al., 2019; Albergo et al., 2019; Nicoli et al., 2019).

NFs can be categorized into two families: (i) Coupling layers (Dinh et al., 2014; 2016; Kingma & Dhariwal, 2018; Müller et al., 2018), which are a subclass of autoregressive flows (Germain et al., 2015; Papamakarios et al., 2017; Huang et al., 2018; De Cao et al., 2019; Durkan et al., 2019), and (ii) residual flows (Chen et al., 2018; Zhang et al., 2018; Grathwohl et al., 2018; Behrmann et al., 2018; Chen et al., 2019) – see (Papamakarios et al., 2019) for an extensive review of flow architectures. There is a trade-off between the expressiveness of flow architectures and the computational cost in training or sampling from them. A major caveat of working with exactly invertible functions are topological constraints (Falorsi et al., 2018; 2019). For example, when trying to map a unimodal Gaussian distribution to a bimodal distribution with a coupling layer flow, a connection between the modes remains (Fig. 1a). Topological constraints pose serious problems during optimization – in the bimodal distribution example, the connection between the density modes seems largely determined by the initialization and does not move during optimization, leading to very different results in multiple runs (Suppl. Fig. 7). Such problems can be reduced by using mixtures of flows (Dinh et al., 2019; Cornish et al., 2019) or augmenting the base space (Dupont et al., 2019) at the cost of limiting expressibility or losing the exact density.

For sampling energy-based models, an alternative to flows is to use Markov Chain Monte Carlo (MCMC) or other stochastic sampling methods (Frenkel & Smit, 2001). This approach is asymptotically unbiased, but suffers from the sampling problem: without knowing efficient moves, MCMC approaches may get stuck in local energy minima for a long time and fail to converge in practice.

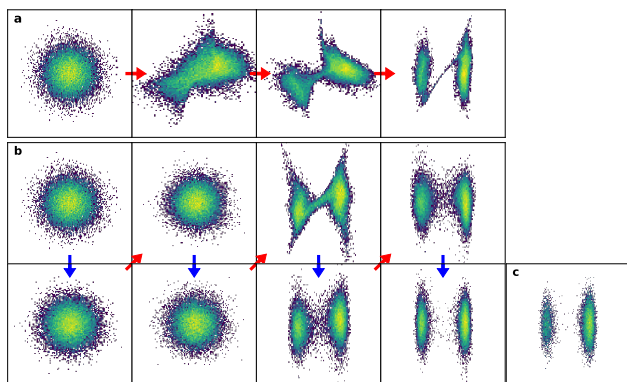


Figure 1. **Deterministic versus stochastic normalizing flow for the double well.** Red arrows indicate deterministic transformations, blue arrows indicate stochastic dynamics. **a)** 3 RealNVP blocks (2 layers each). **b)** Same with 20 BD steps before or after RealNVP blocks. **c)** Unbiased sample from true distribution.

Contributions Here we introduce Stochastic Normalizing Flows (SNF), a marriage between NFs and stochastic sampling. SNFs significantly generalize flow architectures as they can consist of an arbitrary sequence of any deterministic flow transformation and any stochastic sampling method with tractable path-likelihood, such as MCMC, Langevin Dynamics or Hamiltonian Monte Carlo (HMC) (Fig. 2). Stochastic sampling helps to overcome topological constraints and improve expressivity of the chosen deterministic flow architecture (Fig. 1b). On the other hand, trainable deterministic flows do the “heavy lifting” of probability transformation (Fig. 1a,b) and can improve sampling efficiency over pure stochastic sampling.

The main challenge using stochastic processes in NFs is that the exact computation of the marginal probability of generated samples becomes intractable as it involves an integral over all random variable realizations. However, we demonstrate that SNFs can be trained without computing exact generation probabilities by invoking ideas from nonequilibrium statistical mechanics. The resulting loss functions are conceptually simple generalizations of the usual KL or ML losses used for normalizing flows. Overall, our main contributions are:

- Introducing the Stochastic Normalizing Flow (SNF) learning framework, and introducing SNF layers for popular stochastic processes.
- Developing training methods for SNFs that avoid computation of the intractable marginal probabilities.
- Computing reweighting factors for SNF samples, leading to sampling without asymptotic bias, turn the SNF into a Boltzmann Generator.

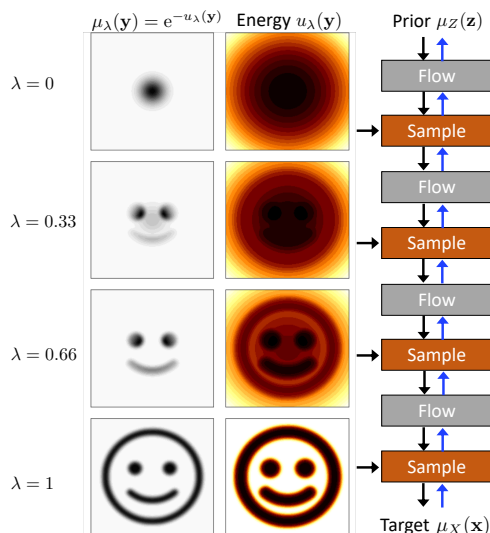


Figure 2. **Schematic for Stochastic Normalizing Flow (SNF).** An SNF transform a tractable prior $\mu_Z(\mathbf{z}) \propto e^{-u_0(\mathbf{z})}$ to a complicated target distribution $\mu_X(\mathbf{x}) \propto e^{-u_1(\mathbf{x})}$ by a sequence of deterministic invertible transformations (flows, grey boxes) and stochastic dynamics (sample, orange) that sample with respect to a guiding potential $u_\lambda(\mathbf{x})$. SNFs can be run in forward mode (black) and reverse mode (blue).

- Demonstrating on benchmark densities and variational inference of images that SNFs can improve representational power of a given deterministic flow architecture while improving statistical efficiency of a given stochastic sampling method.
- Improving the state-of-the-art for the energy-based generation of molecular structures with flows.

Related work A cornerstone of our work is nonequilibrium statistical mechanics. Particularly important is Nonequilibrium Candidate Monte Carlo (NCMC) (Nilmeier et al., 2011), which provides the theoretical framework to compute SNF path likelihood ratios. However, NCMC is for fixed deterministic and stochastic protocols, while we derive a machine learning structure.

Neural stochastic differential equations learn stochastic processes from observations along the path (Tzen & Raginsky, 2019; Jia & Benson, 2019; Liu et al., 2019; Li et al., 2020), but are not designed for marginal density estimation or asymptotically unbiased sampling. It has been demonstrated that combining learnable proposals/transformations with stochastic sampling techniques can improve expressiveness of the proposals (Salimans et al., 2015; Levy et al., 2017; Song et al., 2017; Hoffman et al., 2019; Hoffman, 2017). However, these contributions do not provide an exact reweighting scheme based on a tractable model likelihood and it remains unclear how to combine arbitrary se-

quences of learnable transformations and sampling steps in trainable way. Nevertheless, these methods can be implemented as instances of SNFs without the trainable deterministic part.

More closely related is (Sohl-Dickstein et al., 2015) which uses of stochastic flows for density estimation and trains diffusion kernels by maximizing a variational bound of the data likelihood. Their derivation using stochastic paths is similar to ours and this work can be seen as a special instance of SNFs, but it does not consider more general stochastic and deterministic building blocks and does not discuss the problem of asymptotically unbiased sampling of a target density. (Chen et al., 2017) propose a learnable stochastic process by integrating Langevin dynamics with learnable drift and diffusion term. While this approach is in spirit similar to our proposed method, it requires variational approximation of the generative distribution using a distillation network and it has not worked out how it could be used as a building block within a NF.

2. Normalizing Flows & Boltzmann Generators

We briefly summarize the framework of normalizing flows and Boltzmann Generators and introduce notation.

Normalizing Flows A normalizing flow is an invertible parametric transformation, usually represented by a neural network, that maps a probability density from latent or “prior” space Z to target space X . We call the entire flow map F_{ZX} and its inverse $F_{XZ} = F_{ZX}^{-1}$. A flow consists of T invertible transformation layers F_0, \dots, F_T and we denote states along the flow \mathbf{y}_t :

$$\mathbf{y}_{t+1} = F_t(\mathbf{y}_t) \quad \mathbf{y}_t = F_t^{-1}(\mathbf{y}_{t+1}) \quad (1)$$

For simplicity we call the samples in Z and X also \mathbf{z} and \mathbf{x} , respectively. Overall, the flow structure is as follows:

$$\mathbf{z} = \mathbf{y}_0 \begin{array}{c} \xrightarrow{F_0} \\ \xleftarrow{F_0^{-1}} \end{array} \mathbf{y}_1 \begin{array}{c} \xrightarrow{\dots} \\ \xleftarrow{\dots} \end{array} \mathbf{y}_{T-1} \begin{array}{c} \xrightarrow{F_{T-1}} \\ \xleftarrow{F_{T-1}^{-1}} \end{array} \mathbf{y}_T = \mathbf{x}$$

We suppose each transformation layer is differentiable with a Jacobian determinant $|\det \mathbf{J}_t(\mathbf{y})|$. Due to invertibility, we can invoke the transformation of random variable formula:

$$p_{t+1}(\mathbf{y}_{t+1}) = p_{t+1}(F_t(\mathbf{y}_t)) = p_t(\mathbf{y}_t) |\det \mathbf{J}_t(\mathbf{y}_t)|^{-1} \quad (2)$$

As we often work with log-densities, we abbreviate the log Jacobian determinant as:

$$\Delta S_t = \log |\det \mathbf{J}_t(\mathbf{y})|.$$

The log Jacobian determinant of the entire flow is defined by $\Delta S_{ZX} = \sum_t \Delta S_t(\mathbf{y}_t)$ and correspondingly ΔS_{XZ} for the inverse flow.

Training of flows employs either of two modes:

1. Density estimation – given data samples \mathbf{x} , train the flow such that the back-transformed samples $\mathbf{z} = F_{XZ}(\mathbf{x})$ follow a simple latent distribution $\mu_Z(\mathbf{z})$.
2. Sampling of a given target density $\mu_X(\mathbf{x})$ – sample from the simple distribution $\mu_Z(\mathbf{z})$ and minimize the difference between the distribution generated by the forward-transformation $\mathbf{x} = F_{ZX}(\mathbf{z})$ and $\mu_X(\mathbf{x})$.

We will use densities interchangeably with energies, defined by the negative logarithm of the density. The exact prior and target distributions are:

$$\mu_Z(\mathbf{z}) = Z_Z^{-1} e^{-u_Z(\mathbf{z})} \quad \mu_X(\mathbf{x}) = Z_X^{-1} e^{-u_X(\mathbf{x})} \quad (3)$$

with generally unknown normalization constants Z_Z and Z_X . We assume that $\mu_Z(\mathbf{z})$ is easy to sample from, usually a Gaussian normal distribution $\mu_Z(\mathbf{z}) = \mathcal{N}(\mathbf{0}, \mathbf{I})$.

Energy-based training and forward weight maximization If the target density μ_X is known up to a constant Z_X , we minimize the forward KL divergence between the generated and the target distribution.

$$\begin{aligned} \text{KL}(p_X \parallel \mu_X) & \quad (4) \\ &= \mathbb{E}_{\mathbf{x} \sim p_X(\mathbf{x})} [\log p_X(\mathbf{x}) - \log \mu_X(\mathbf{x})] \\ &= \mathbb{E}_{\mathbf{z} \sim \mu_Z(\mathbf{z})} [u_X(F_{ZX}(\mathbf{z})) - \Delta S_{ZX}(\mathbf{z})] + \text{const} \end{aligned}$$

The importance weights wrt the target distribution can be computed as:

$$w_X(\mathbf{x}) = \frac{\mu_X(\mathbf{x})}{p_X(\mathbf{x})} \propto e^{-u_X(F_{ZX}(\mathbf{z})) + u_Z(\mathbf{z}) + \Delta S_{ZX}(\mathbf{z})} \quad (5)$$

As $\mathbb{E}_{\mathbf{z} \sim p_Z(\mathbf{z})} [u_Z(\mathbf{z})]$ is a constant, we can equivalently minimize KL or maximize log weights:

$$\max \mathbb{E}_{\mathbf{z} \sim p_Z(\mathbf{z})} [\log w_X(\mathbf{x})] = \min \text{KL}(p_X \parallel \mu_X), \quad (6)$$

Maximum likelihood and backward weight maximization The backward KL divergence $\text{KL}(\mu_X \parallel p_X)$ is not always tractable as $\mu_X(\mathbf{x})$ can be difficult to sample from. Replacing $\mu_X(\mathbf{x})$ by the empirical data distribution $\rho_X(\mathbf{x})$, the KL becomes a negative log-likelihood:

$$\begin{aligned} \text{NLL}(\rho_X \parallel p_X) & \quad (7) \\ &= \mathbb{E}_{\mathbf{x} \sim \rho_X(\mathbf{x})} [u_Z(F_{XZ}(\mathbf{x})) - \Delta S_{XZ}(\mathbf{x})] + \text{const} \end{aligned}$$

Using $\mathbb{E}_{\mathbf{x} \sim \rho_X(\mathbf{x})} [-\log \rho_X(\mathbf{x})] = \text{const}$ and the weights:

$$w_Z(\mathbf{z}) = \frac{\mu_Z(\mathbf{z})}{p_Z(\mathbf{z})} \propto e^{-u_Z(F_{XZ}(\mathbf{x})) - \log \rho_X(\mathbf{x}) + \Delta S_{XZ}(\mathbf{x})},$$

maximum likelihood equals log weight maximization:

$$\max \mathbb{E}_{\mathbf{x} \sim \rho_X(\mathbf{x})} [\log w_Z(\mathbf{z})] = \min \text{NLL}(\rho_X \parallel p_X), \quad (8)$$

Boltzmann Generators A Boltzmann Generator is a combination of (i) a flow to generate one-shot samples $\mathbf{x} \sim p_X(\mathbf{x})$ and (ii) a reweighting or resampling procedure respecting the weights $w_X(\mathbf{x})$ that turns these one-shot samples into asymptotically unbiased samples. In the statistical limit a Boltzmann Generator samples $\mathbf{x} \sim \mu_X(\mathbf{x})$ unbiased for all \mathbf{x} it can generate (Noé et al., 2019) – note that in practice, ensuring ergodicity, i.e. sampling all relevant modes of \mathbf{x} , requires combining flow training with a sampling method that can explore new states. Unbiased sampling is particularly important for applications in physics and chemistry where unbiased expectation values are required (Li & Wang, 2018; Noé et al., 2019; Albergo et al., 2019; Nicoli et al., 2019). Two basic reweighting/resampling methods are:

1. **Importance sampling** (Müller et al., 2018; Noé et al., 2019): Generate $\mathbf{x}_k \sim p_X(\mathbf{x})$ and compute observables of interest as

$$\mathbb{E}_{\mu_X}[O] \approx \frac{\sum_k w_X(\mathbf{x}_k) O(\mathbf{x}_k)}{\sum_k w_X(\mathbf{x}_k)}. \quad (9)$$

2. **Neural MCMC** (Li & Wang, 2018; Albergo et al., 2019; Nicoli et al., 2019): Generate a chain $\mathbf{x}_k^{\text{prop}} \sim p_X(\mathbf{x})$ with $k = 1 \dots K$. Set $\mathbf{x}_0 = \mathbf{x}_0^{\text{prop}}$. For $k \geq 1$ sample $u_k \sim \text{uniform}(0, 1)$ and set:

$$\mathbf{x}_k = \begin{cases} \mathbf{x}_k^{\text{prop}} & u_k < \max \left\{ 1, \frac{w_X(\mathbf{x}_k^{\text{prop}})}{w_X(\mathbf{x}_{k-1})} \right\} \\ \mathbf{x}_{k-1} & \text{else.} \end{cases}$$

3. Stochastic normalizing flows

General flow layer We introduce a general flow transformation that may be implemented using any known invertible deterministic transformation or using any stochastic process with a tractable path density. For the forward transformation, we sample the new state \mathbf{y}_{t+1} conditioned on the input \mathbf{y}_t using the conditional forward path density q_t , and vice versa for the backward transform using the conditional backward path density \tilde{q}_t .

$$\mathbf{y}_{t+1} | \mathbf{y}_t \sim q_t(\mathbf{y}_t \rightarrow \mathbf{y}_{t+1}) \quad (10)$$

$$\mathbf{y}_t | \mathbf{y}_{t+1} \sim \tilde{q}_t(\mathbf{y}_{t+1} \rightarrow \mathbf{y}_t) \quad (11)$$

We also need a generalization of the Jacobian. The SNF layer defined by forward and backward steps (10-11) scales probability volume by the factor $e^{\Delta S_t}$ with:

$$\Delta S_t = -\Delta \tilde{S}_t = \log \frac{\tilde{q}_t(\mathbf{y}_{t+1} \rightarrow \mathbf{y}_t)}{q_t(\mathbf{y}_t \rightarrow \mathbf{y}_{t+1})}, \quad (12)$$

$\Delta \tilde{S}_t$ is the log-probability of the reverse realization. ΔS_t can be interpreted as the entropy in the variational free energy of the flow transformation (Noé et al., 2019; Li & Wang, 2018). We consider the following two cases of q_t :

1. **Deterministic step:** q_t is defined by a trainable deterministic flow transformation $\mathbf{y}_{t+1} = F_t(\mathbf{y}_t)$ and \tilde{q}_t by its inverse F_t^{-1} . Formally:

$$\begin{aligned} \mathbf{y}_{t+1} &= \delta(\mathbf{y}_{t+1} - F_t(\mathbf{y}_t)) \\ \mathbf{y}_t &= \delta(\mathbf{y}_t - F_t^{-1}(\mathbf{y}_{t+1})) \end{aligned}$$

For this choice, ΔS_t equals the log Jacobian of the transformation $\Delta S_t = \log |\det \mathbf{J}_t(\mathbf{y}_t)|$ (Section 4).

2. **Stochastic step:** q_t is defined by a stochastic process, e.g., MCMC. The backward process \tilde{q}_t is identical to the forward process, only if the stochastic process involves velocities (e.g., Langevin dynamics), \tilde{q}_t propagates the state with inverted velocities. $e^{\Delta S_t}$ equals the probability ratio of realizing the backward and forward paths. The protocols q_t and \tilde{q}_t must be chosen such that ΔS_t is always finite, i.e. for any forward transition, the corresponding backward transition must have finite probability, and vice versa.

An SNF is a sequence of such transformation layers (Fig. 2). We sample the $\mathbf{z} = \mathbf{y}_0$ from the prior μ_Z , and the forward path $(\mathbf{y}_1, \dots, \mathbf{y}_T)$ is generated by executing the T stochastic and deterministic transformations. Correspondingly, a latent space sample can be generated by starting from a sample $\mathbf{x} = \mathbf{y}_T$ and invoking the backward path $(\mathbf{y}_{T-1}, \dots, \mathbf{y}_0)$. The conditional forward and backward path probabilities are

$$\mathbb{P}_f(\mathbf{z} = \mathbf{y}_0 \rightarrow \mathbf{x} = \mathbf{y}_T) = \prod_{t=0}^{T-1} q_t(\mathbf{y}_t \rightarrow \mathbf{y}_{t+1}) \quad (13)$$

$$\mathbb{P}_b(\mathbf{x} = \mathbf{y}_T \rightarrow \mathbf{y}_0 = \mathbf{z}) = \prod_{t=0}^{T-1} \tilde{q}_t(\mathbf{y}_{t+1} \rightarrow \mathbf{y}_t) \quad (14)$$

Training Stochastic Normalizing Flows While in deterministic normalizing flows, the probability of generating a sample \mathbf{x} can be computed by Eq. (2), this is not possible for SNFs. The marginal probability of generating \mathbf{x} involves integrating over all paths that end in \mathbf{x} :

$$p_X(\mathbf{x}) = \int \mu_Z(\mathbf{y}_0) \mathbb{P}_f(\mathbf{y}_0 \rightarrow \mathbf{y}_T) d\mathbf{y}_0 \dots d\mathbf{y}_{T-1}. \quad (15)$$

As this integral is generally intractable, the key problem for SNFs is to find a training method that avoids Eq. (15).

We first give the results and show derivations below. Surprisingly, SNFs can be trained using only random path samples – we only have to use the more general log probability ratio W_t instead of the log Jacobian determinant. In energy-based training, we use the flow in forward mode and train it to sample a given target density $\mathbf{x} \sim \mu_X(\mathbf{x})$:

$$J_{KL} = \mathbb{E}_{\mathbf{z} \sim \mu_Z, \mathbf{y}_1, \dots, \mathbf{y}_T} \left[u_X(\mathbf{y}_T) - \sum_{t=0}^{T-1} \Delta S_t \right]. \quad (16)$$

Likelihood maximization (density estimation) is performed by running the SNF in backward mode and feeding it with samples \mathbf{x} from the data distribution ρ_X :

$$J_{ML} = \mathbb{E}_{\mathbf{x} \sim \rho_X, \mathbf{y}_{T-1}, \dots, \mathbf{y}_0} \left[u_Z(\mathbf{y}_0) - \sum_{t=0}^{T-1} \Delta \tilde{S}_t \right] \quad (17)$$

For training we can then combine both losses with a mixing constant $c \in [0, 1]$, $J = cJ_{KL} + (1 - c)J_{ML}$ (Noé et al., 2019). These loss functions can be derived and interpreted in two different ways, either by viewing paths $\mathbf{z} \rightarrow \mathbf{x}$ in the framework of nonequilibrium statistical mechanics or by following a variational bound, as shown below.

Derivation via weight maximization If we draw samples in latent space via $\mathbf{z} \sim \mu_Z(\mathbf{z})$ and transform them to samples \mathbf{x} through the SNF, a sufficient condition to sample $\mathbf{x} \sim \mu_X(\mathbf{x})$ is to respect path-based detailed balance:

$$\mu_Z(\mathbf{z}) \mathbb{P}_f(\mathbf{z} \rightarrow \mathbf{x}) A(\mathbf{z} \rightarrow \mathbf{x}) = \mu_X(\mathbf{x}) \mathbb{P}_b(\mathbf{x} \rightarrow \mathbf{z}) A(\mathbf{x} \rightarrow \mathbf{z})$$

This can be achieved by running MCMC in path-space and accepting paths with the ratio (Nilmeier et al., 2011)

$$\frac{A(\mathbf{z} \rightarrow \mathbf{x})}{A(\mathbf{x} \rightarrow \mathbf{z})} = \frac{\mu_X(\mathbf{x}) \mathbb{P}_b(\mathbf{x} \rightarrow \mathbf{z})}{\mu_Z(\mathbf{z}) \mathbb{P}_f(\mathbf{z} \rightarrow \mathbf{x})}. \quad (18)$$

As we sample paths independently, it is simpler to assign an unnormalized importance weight proportional to the acceptance ratio to each sample path $\mathbf{z} = \mathbf{y}_0, \dots, \mathbf{y}_T = \mathbf{x}$. Inserting Equations (3, 12, 13, 14) into (18):

$$w(\mathbf{z} \rightarrow \mathbf{x}) = e^{-u_X(\mathbf{x}) + u_Z(\mathbf{z}) + \sum_t \Delta S_t(\mathbf{y}_t)} \quad (19)$$

Now, the natural training method is weight maximization (Eq. 6 and 8). With Eq. (19), it immediately follows that maximizing $\mathbb{E}_{\mathbf{z} \sim \mu_Z, \mathbf{y}_1, \dots, \mathbf{y}_T = \mathbf{x}} [\log w(\mathbf{z} \rightarrow \mathbf{x})]$ equals minimizing the energy-based loss Eq. (16). For likelihood-based training we use the reverse path weight $w(\mathbf{x} \rightarrow \mathbf{z})$ and can analogously derive Eq. (17).

Derivation as a variational bound In the second derivation, we first use the fact that the KL divergence between two joint distributions is an upper bound to the KL divergence between the marginal distributions:

$$\begin{aligned} & \text{KL}(p_X(\mathbf{x}) \parallel \mu_X(\mathbf{x})) \\ & \leq \text{KL}(\mu_Z(\mathbf{z}) \mathbb{P}_f(\mathbf{z} \rightarrow \mathbf{x}) \parallel \mu_X(\mathbf{x}) \mathbb{P}_b(\mathbf{x} \rightarrow \mathbf{z})) \end{aligned} \quad (20)$$

Note that invoking this variational approximation does *not* preclude us from generating asymptotically unbiased samples from the target density μ_X , unlike in variational inference. Using Equations (13-14) it follows that minimizing the upper bound in Eq. (20) equals minimization of Eq. (16). Likewise we can confirm the log-likelihood loss

Eq. (17). For this, we use the variational bound (20) on $\text{KL}(\mu_X(\mathbf{x}) \parallel p_X(\mathbf{x}))$, and arrive at a path-based reversed KL divergence as above. Replacing the exact distribution μ_X by the data distribution ρ_X then yields the maximum likelihood loss (17).

Reweighting – SNF as Boltzmann Generator We can turn an SNF into a Boltzmann Generator and generate asymptotically unbiased samples of $\mathbf{x} \sim \mu_X(\mathbf{x})$ by performing importance sampling or Neural MCMC using the path weights $w(\mathbf{z}_k \rightarrow \mathbf{x}_k)$ (Eq. 19) for each path sample k . An asymptotically unbiased estimator of the expectation values of function O is (Proof in Suppl. Material):

$$\mathbb{E}_{\mu_X}[O] \approx \frac{\sum_{k=1} w(\mathbf{z}_k \rightarrow \mathbf{x}_k) O(\mathbf{x}_k)}{\sum_{k=1} w(\mathbf{z}_k \rightarrow \mathbf{x}_k)} \quad (21)$$

4. Stochastic Normalizing Flow Layers

We now describe practical implementations of SNFs. Below we describe common choices of stochastic samplers and compute their log path probability ratio ΔS_t to render them readily usable as SNF layers. In this paper we focus on the use of SNFs as samplers of $\mu_X(\mathbf{x})$ for problems where the target energy $u_X(\mathbf{x})$ is known, defining the target density up to a constant. SNF layers such as MCMC or Langevin dynamics typically make local stochastic updates of the current state \mathbf{y} with respect to some potential $u_\lambda(\mathbf{y})$ such that they will asymptotically sample from $\mu_\lambda(\mathbf{y}_t) \propto e^{-u_\lambda(\mathbf{y}_t)}$. While the potentials $u_\lambda(\mathbf{y})$ can be learned, a straightforward strategy is to interpolate them between the prior and target potentials:

$$u_\lambda(\mathbf{y}) = (1 - \lambda)u_Z(\mathbf{y}) + \lambda u_X(\mathbf{y}).$$

These potentials “guide” the sampling in each SNF layer, similar as in annealed importance sampling (Neal, 1998). Thus, deterministic flow layers only have to approximate the partial density transformation between adjacent λ steps while the stochastic flow layers can anneal wrt to the given potential u_λ . Thus, the u_λ are key in making SNF training and sampling robust. λ could again be learned or be simply chosen as a linear interpolation along the SNF layers: $\lambda = t/T$.

Deterministic Flow layers We can implement the deterministic flow transformations in Fig. 2 with any invertible differentiable transformation, such as NICE (Dinh et al., 2014), RealNVP (Dinh et al., 2016), invertible ResNets (Behrmann et al., 2018) or neural ODEs (Chen et al., 2018) – see (Papamakarios et al., 2019) for an overview of flow architectures. For deterministic transformations the log path probability ratio simply equals the Jacobian of the transformation (Suppl. Material):

$$\Delta S_t = \log |\det \mathbf{J}_t(\mathbf{y}_t)|.$$

Overdamped Langevin dynamics, also known as Brownian using an Euler discretization with time step Δt is given by (Ermak & Yeh, 1974):

$$\mathbf{y}_{t+1} = \mathbf{y}_t - \epsilon_t \nabla u_\lambda(\mathbf{y}_t) + \sqrt{\frac{2\epsilon_t}{\beta}} \boldsymbol{\eta}_t \quad (22)$$

where $p(\boldsymbol{\eta}_t) = \mathcal{N}(0, \mathbf{I})$. In physical systems, the constant ϵ_t has the form $\epsilon_t = \frac{\Delta t}{\gamma m}$ with time step Δt , friction coefficient γ and mass m , and β is the inverse temperature (here set to 1). The backward step $\mathbf{y}_{t+1} \rightarrow \mathbf{y}_t$ is realized under these dynamics with the backward noise realization (Suppl. Material), (Nilmeier et al., 2011):

$$\tilde{\boldsymbol{\eta}}_t = \sqrt{\frac{\beta \epsilon_t}{2}} [\nabla u_\lambda(\mathbf{y}_t) + \nabla u_\lambda(\mathbf{x}_{t+1})] - \boldsymbol{\eta}_t$$

The log path probability ratio is (Suppl. Material):

$$\Delta S_t = -\frac{1}{2} \left(\|\tilde{\boldsymbol{\eta}}_t\|^2 - \|\boldsymbol{\eta}_t\|^2 \right)$$

Langevin dynamics When not being in the overdamped limit, Langevin dynamics propagates positions and velocities $\mathbf{y}_t = (\mathbf{x}_t, \mathbf{v}_t)$ by Newtonian dynamics with additional friction and a stochastic force from a heat bath. The forward step $(\mathbf{x}_t, \mathbf{v}_t) \rightarrow (\mathbf{x}_{t+1}, \mathbf{v}_{t+1})$ using the leap frog integrator is defined by (Brünger et al., 1984):

$$\begin{aligned} \mathbf{v}' &= \mathbf{v}_t + \frac{\Delta t}{2m} \left[-\nabla u_\lambda(\mathbf{x}_t) - \gamma m \mathbf{v}_t + \sqrt{\frac{4\gamma m}{\Delta t \beta}} \boldsymbol{\eta}_t \right] \\ \mathbf{x}_{t+1} &= \mathbf{x}_t + \Delta t \mathbf{v}' \\ \mathbf{v}_{t+1} &= \frac{1}{1 + \frac{\gamma \Delta t}{2}} \left[\mathbf{v}' + \frac{\Delta t}{2m} \left(-\nabla u_\lambda(\mathbf{x}_{t+1}) + \sqrt{\frac{4\gamma m}{\Delta t \beta}} \boldsymbol{\eta}'_t \right) \right], \end{aligned}$$

where $p(\boldsymbol{\eta}_t) = p(\boldsymbol{\eta}'_t) = \mathcal{N}(0, \mathbf{I})$. The reverse step is defined by $(\mathbf{x}_{t+1}, -\mathbf{v}_{t+1}) \rightarrow (\mathbf{x}_t, -\mathbf{v}_t)$ and is realized by the noise variables (Nilmeier et al., 2011):

$$\tilde{\boldsymbol{\eta}}_t = \boldsymbol{\eta}'_t - \sqrt{\frac{\gamma \Delta t m}{k_B T}} \mathbf{v}_{t+1} \quad \tilde{\boldsymbol{\eta}'_t} = \boldsymbol{\eta}_t - \sqrt{\frac{\gamma \Delta t m}{k_B T}} \mathbf{v}_t$$

The log path probability ratio is (Suppl. Material):

$$\Delta S_t = -\frac{1}{2} \left(\left(\|\tilde{\boldsymbol{\eta}}_t\|^2 + \|\tilde{\boldsymbol{\eta}'_t}\|^2 \right) - \left(\|\boldsymbol{\eta}_t\|^2 + \|\boldsymbol{\eta}'_t\|^2 \right) \right)$$

Markov Chain Monte Carlo In MCMC, we propose a new state by sampling from a proposal density $g_t(\mathbf{y}^* | \mathbf{y}_t)$.

$$\mathbf{y}^* \sim g_t(\mathbf{y}^* | \mathbf{y}_t)$$

To achieve equilibrium sampling in the potential $u_\lambda(\mathbf{y})$ we accept the proposed state according to a criterion that ensures detailed balance with respect to the equilibrium density $e^{-u_\lambda(\mathbf{y})}$. A popular choice is the Metropolis-Hastings scheme with $w_t \sim \text{uniform}(0, 1)$:

$$\mathbf{y}_{t+1} = \begin{cases} \mathbf{y}^* & w_t \leq \min \left\{ 1, e^{-(u_\lambda(\mathbf{y}^*) - u_\lambda(\mathbf{y}_t))} \frac{g_t(\mathbf{y}_t | \mathbf{y}^*)}{g_t(\mathbf{y}^* | \mathbf{y}_t)} \right\} \\ \mathbf{y}_t & \text{else,} \end{cases}$$

The log path probability ratio is (Suppl. Material):

$$\Delta S_t = \begin{cases} u_\lambda(\mathbf{y}_{t+1}) - u_\lambda(\mathbf{y}_t) + \log \frac{g_t(\mathbf{y}_t | \mathbf{y}_{t+1})}{g_t(\mathbf{y}_{t+1} | \mathbf{y}_t)} & \text{if accept} \\ 0 & \text{if reject} \end{cases}$$

For symmetric proposals, such as in traditional Metropolis MC this is always $\Delta S_t = u_\lambda(\mathbf{y}_{t+1}) - u_\lambda(\mathbf{y}_t)$.

Hamiltonian MC with Metropolis acceptance In Hamiltonian MC (HMC) we sample auxiliary variables (velocities) $\mathbf{v} \sim \mathcal{N}(\mathbf{0}, \boldsymbol{\Sigma})$, and propagate $\mathbf{y}_t^0 = \mathbf{y}_t$ with the leap frog integrator in K steps $k = 0, \dots, K - 1$:

$$\begin{aligned} \mathbf{v}^{k+\frac{1}{2}} &= \mathbf{v}^k - \frac{\epsilon_t}{2} \nabla u_\lambda(\mathbf{y}^k) \\ \mathbf{y}^{k+1} &= \mathbf{y}^k + \epsilon_t \boldsymbol{\Sigma}^{-1} \mathbf{v}^{k+\frac{1}{2}} \\ \mathbf{v}^{k+1} &= \mathbf{v}^{k+\frac{1}{2}} - \frac{\epsilon_t}{2} \nabla u_\lambda(\mathbf{y}^{k+1}) \end{aligned}$$

with a constant ϵ_t . To ensure equilibrium sampling in the potential $u_\lambda(\mathbf{y})$ we compute the new state via a Metropolis acceptance step with $w_t \sim \text{uniform}(0, 1)$:

$$\mathbf{y}_{t+1} = \begin{cases} \mathbf{y}^K & w_t \leq \min \left\{ e^{u_\lambda(\mathbf{y}_t) - u_\lambda(\mathbf{y}^K)} \frac{\mathcal{N}(\mathbf{v}^K | \mathbf{0}, \boldsymbol{\Sigma})}{\mathcal{N}(\mathbf{v} | \mathbf{0}, \boldsymbol{\Sigma})}, 1 \right\} \\ \mathbf{y}_t & \text{else.} \end{cases}$$

The log path probability ratio is:

$$\Delta S_t = \begin{cases} \log \frac{\mathcal{N}(\mathbf{v}^K | \mathbf{0}, \boldsymbol{\Sigma})}{\mathcal{N}(\mathbf{v} | \mathbf{0}, \boldsymbol{\Sigma})} & \text{if accept} \\ 0 & \text{if reject.} \end{cases}$$

5. Results

Representational power versus sampling efficiency

We first illustrate that SNFs can break topological constraints and improve the representational power of deterministic normalizing flows and at the same time beat direct MCMC in terms of sampling efficiency. To this end we use images to define complex two-dimensional densities (Fig. 3, ‘‘Exact’’) as target densities $\mu_X(\mathbf{x})$ to be sampled. Note that a benchmark aiming at generating high-quality images would instead represent the image as a high-dimensional pixel array. We compare three flows with 5 blocks each trained by samples from the exact density: (i) a normalizing flow with 2 swapped RealNVP layers per block, (ii) a non-trainable stochastic flow with 10 Metropolis MC steps per block, (iii) a SNF with both, 2 swapped RealNVP layers and 10 Metropolis MC steps per block (Details in Suppl. Material).

The RealNVP normalizing flow architecture chosen here has limited representational power, resulting in a ‘‘smeared out’’ image that does not resolve detailed structures (Fig. 3, RNVP). The pure Metropolis MC flow suffers from sampling problems – density is still concentrated in the image center from the prior. Many more MC steps would be

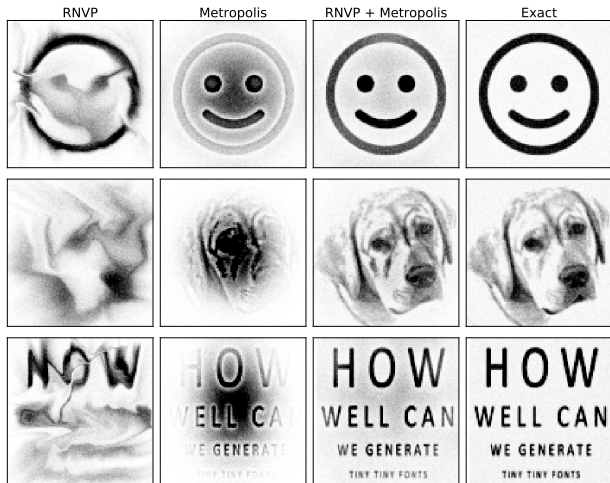


Figure 3. **Sampling of two-dimensional densities.** Columns: (1) Normalizing Flow with RealNVP layers, (2) Metropolis MC sampling, (3) Stochastic Normalizing Flow combining (1+2), (4) Unbiased sample from exact density.

needed to converge to the exact density (see below). The SNF achieves high-quality approximations despite it simply combines the same deterministic and stochastic flow components that fail individually (RNVP, Metropolis) in the SNF learning framework (Fig. 3, RNVP+Metropolis). This indicates that the SNF succeeds in performing the large-scale probability mass transport with the trainable flow layers and sampling the details with MetropolisMC.

Fig. 4 quantifies these impressions by computing the KL divergence between generated densities $p_X(\mathbf{x})$ and exact densities $\mu_X(\mathbf{x})$. Both normalizing flows and SNFs improve with greater depth, but SNFs achieve significantly lower KL divergence at a fixed network depth. Moreover, SNFs have higher statistical efficiency than pure Metropolis MC flows. Depending on the example, 1-2 orders of magnitude more Metropolis MC steps are needed to achieve similar KL divergence as with an SNF. This demonstrates that the large-scale probability transport learned by the trainable deterministic flow blocks in SNFs significantly helps with the sampling.

SNFs as Boltzmann Generators We demonstrate that SNFs can be used to sample target densities without asymptotic bias by revisiting the two-well example (Fig. 1). Fig. 5a (black) shows the free energies (negative marginal density) along the double-well coordinate x_1 . Flows with 3 RealNVP blocks are trained with a mixed loss $J = \frac{1}{2}J_{KL} + \frac{1}{2}J_{ML}$ using either data from a biased distribution, or with the unbiased distribution (Details in Suppl. Material). Even when training with the unbiased distribution, the generation probability $p_X(\mathbf{x})$ will be biased due to limitations in representational power. We use importance

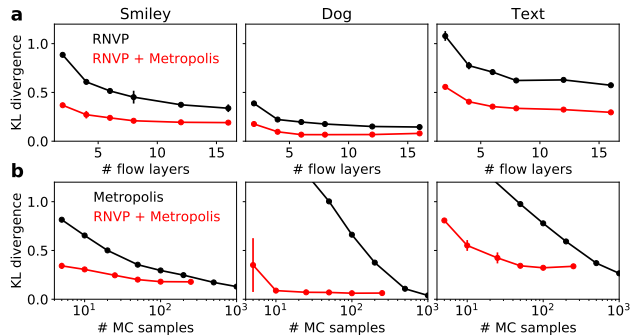


Figure 4. **Representative power and statistical efficiency of stochastic normalizing flows.** KL divergence (mean and standard deviation over 3 training runs) between flow samples and true density for the three images (“smiley”, “dog”, “text”) from Fig. 3. **a)** Comparison of deterministic flow (black) and SNF (red) as a function of the number of RealNVP transformations. Number of MC steps in SNF is fixed to 50. **b)** Comparison of pure Metropolis MC (black) and SNF (red) as a function of the number of MC steps. Number of RealNVP transformations in SNF is fixed to 10.

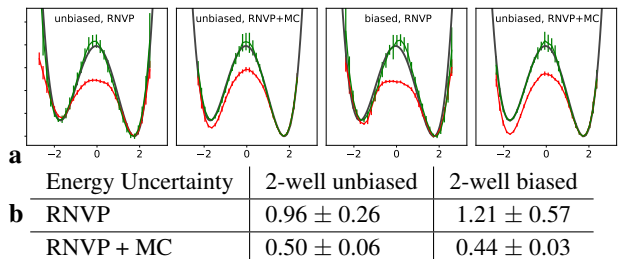


Figure 5. **Reweighting results for the double well potential** (see also Fig. 1). **a)** free energy along x_1 (negative log of marginal density) for deterministic normalizing flows (RNVP) and SNFs (RNVP+MC). Black: exact energy, red: energy of proposal density $p_X(\mathbf{x})$, green: reweighted energy using importance sampling. **b)** Mean uncertainty of the reweighted energy along x_1 averaged over 5 independent runs (\pm standard deviation).

sampling (Eq. 9 and 21) to turn the flows into Boltzmann Generators. Indeed all generator densities $p_X(\mathbf{x})$ can be reweighted to an estimate of the unbiased density $\mu_X(\mathbf{x})$ whose free energies are within statistical error of the exact result (Fig. 5a, red and green).

We rank statistical efficiencies by comparing the statistical uncertainty of the reweighted free energy using a fixed number of samples (20,000). Using SNFs with MetropolisMC steps, uncertainties are reduced by half or more (Fig. 5b). Remarkably, the differences between multiple runs (see standard deviations of the uncertainty estimate) reduce even more, i.e. SNF results are more reproducible than RealNVP flows, confirming that the training problems caused by the density connection between both modes (Fig. 1, Suppl. Fig. 7) can be reduced.

Alanine dipeptide To demonstrate a higher-dimensional example we compare the density estimation and sampling of molecular structures from a simulation of the alanine dipeptide molecule in an implicit solvent model (Fig. 6). The molecule has 66 dimensions in \mathbf{x} , and we augment it with 66 auxiliary dimensions in a second channel \mathbf{v} , similar to “velocities” in a Hamiltonian flow framework (Toth et al., 2019), resulting in 132 dimensions total. The target density is given by $\mu_X(\mathbf{x}, \mathbf{v}) = e^{-u(\mathbf{x}) - \frac{1}{2}\|\mathbf{v}\|^2}$, where $u(\mathbf{x})$ is the potential energy of the molecule and $\frac{1}{2}\|\mathbf{v}\|^2$ is the kinetic energy term. μ_Z is an isotropic Gaussian normal distribution in all dimensions. We utilize the invertible coordinate transformation layer introduced in (Noé et al., 2019) in order to transform \mathbf{x} into normalized bond, angle and torsion coordinates. RealNVP transformations act between the \mathbf{x} and \mathbf{v} variable groups (Detail in Suppl. Material).

We compare deterministic normalizing flows using 5 blocks of 2 RealNVP layers with SNFs that additionally use 20 Metropolis MC steps in each block. Fig. 6a shows random structures sampled by the trained SNF. Fig. 6b shows marginal densities in all five multimodal torsion angles (backbone angles ϕ , ψ and methyl rotation angles γ_1 , γ_2 , γ_3). While the RealNVP networks that are state of the art for this problem miss many of the modes, the SNF resolves the multimodal structure and approximates the target distribution better, as quantified in the KL divergence between the generated and target marginal distributions (Fig. 6b). The SNF achieves these results with only 100 Metropolis MC steps.

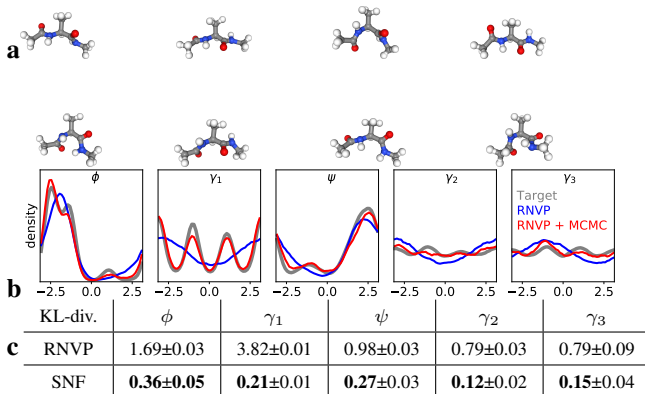


Figure 6. Alanine dipeptide sampled with deterministic normalizing flows and stochastic normalizing flows. **a)** One-shot SNF samples of alanine dipeptide structures. **b)** Energy (negative logarithm) of marginal densities in 5 unimodal torsion angles (top) and all 5 multimodal torsion angles (bottom). **c)** KL-divergences of RNVP flow and SNF (RNVP+MCMC) between generated and target distributions for all multimodal torsion angles. Mean and standard deviation from 3 independent runs.

Variational Inference Finally, we use normalizing flows to model the latent space distribution of a variational autoencoder (VAE) in order to improve variational inference, as suggested in (Rezende & Mohamed, 2015). Table 1 shows results for the variational bound and the log likelihood of the test set for MNIST (LeCun et al., 1998) and Fashion-MNIST (Xiao et al., 2017). The experiments are in 50-dimensional latent spaces and use flows with 3 blocks, each containing 2 swapped RealNVP layers (RNVP), 30 overdamped MCMC steps using overdamped Langevin dynamics as a proposal step (MCMC) or both for the SNF (RNVP+MCMC) (Details in Suppl. Material). For the chosen VAE and flow architectures, employing any kind of flow improves the result over a pure VAE, while the SNF outperforms both, the purely deterministic and the purely stochastic flow.

	MNIST		Fashion-MNIST	
	J_{KL}	NLL	J_{KL}	NLL
VAE	108.4±24.3	98.1±4.2	241.3±7.4	238.0±2.9
RNVP	91.8±0.4	87.0±0.2	233.7±0.1	231.4±0.2
MCMC	102.1±8.0	96.2±1.9	234.7±0.4	235.2±2.4
SNF	89.7±0.1	86.8±0.1	232.4±0.2	230.9±0.2

Table 1. Variational inference using stochastic normalizing flows. J_{KL} : variational bound of the KL-divergence computed during training. NLL: negative log likelihood of test set. SNF uses RNVP and MCMC.

6. Conclusions

We have introduced stochastic normalizing flows (SNFs) that combine both stochastic processes and invertible deterministic transformations into a single learning framework that can be trained to learn densities from data or sample target densities. Key was to formulate flow training only using path samples and avoiding the intractable marginalization of stochastic paths. These results can be motivated either with nonequilibrium statistical mechanics or with a variational bound. Importantly, samples from the flow trained in this manner can still be reweighted to asymptotically unbiased samples of the target density, which is not the case for other variational inference methods such as VAEs. Future directions will include the efficient implementation of SNFs with many stochastic sampling steps and large-scale applications. Besides their applications in classical machine learning domains such as variational and Bayesian inference, we believe that SNFs will be a key component in the efficient sampling of many-body physics systems.

References

- Albergo, M. S., Kanwar, G., and Shanahan, P. E. Flow-based generative models for markov chain monte carlo in lattice field theory. *Phys. Rev. D*, 100:034515, 2019. 1, 2, 2
- Behrmann, J., Grathwohl, W., Chen, R. T., Duvenaud, D., and Jacobsen, J.-H. Invertible residual networks. *arXiv preprint arXiv:1811.00995*, 2018. 1, 4
- Berg, R. v. d., Hasenclever, L., Tomczak, J. M., and Welling, M. Sylvester normalizing flows for variational inference. *arXiv preprint arXiv:1803.05649*, 2018. 1
- Brünger, A., Brooks III, C. L., and Karplus, M. Stochastic boundary conditions for molecular dynamics simulations of st2 water. *Chem. Phys. Lett.*, 105:495–500, 1984. 4
- Chen, C., Li, C., Chen, L., Wang, W., Pu, Y., and Carin, L. Continuous-time flows for efficient inference and density estimation. *arXiv preprint arXiv:1709.01179*, 2017. 1
- Chen, T. Q., Rubanova, Y., Bettencourt, J., and Duvenaud, D. K. Neural ordinary differential equations. In *Advances in neural information processing systems*, pp. 6571–6583, 2018. 1, 4
- Chen, T. Q., Behrmann, J., Duvenaud, D. K., and Jacobsen, J.-H. Residual flows for invertible generative modeling. In *Advances in Neural Information Processing Systems*, pp. 9913–9923, 2019. 1
- Cornish, R., Caterini, A. L., Deligiannidis, G., and Doucet, A. Localised generative flows. *arXiv preprint arXiv:1909.13833*, 2019. 1
- De Cao, N., Titov, I., and Aziz, W. Block neural autoregressive flow. *arXiv preprint arXiv:1904.04676*, 2019. 1
- Dinh, L., Krueger, D., and Bengio, Y. Nice: Non-linear independent components estimation. *arXiv preprint arXiv:1410.8516*, 2014. 1, 4
- Dinh, L., Sohl-Dickstein, J., and Bengio, S. Density estimation using real nvp. *arXiv:1605.08803*, 2016. 1, 4, 6
- Dinh, L., Sohl-Dickstein, J., Pascanu, R., and Larochelle, H. A rad approach to deep mixture models. *arXiv preprint arXiv:1903.07714*, 2019. 1
- Dupont, E., Doucet, A., and Teh, Y. W. Augmented neural odes. In *Advances in Neural Information Processing Systems*, pp. 3134–3144, 2019. 1
- Durkan, C., Bekasov, A., Murray, I., and Papamakarios, G. Neural spline flows. In *Advances in Neural Information Processing Systems*, pp. 7509–7520, 2019. 1
- Ermak, D. L. and Yeh, Y. Equilibrium electrostatic effects on the behavior of polyions in solution: polyion-mobile ion interaction. *Chem. Phys. Lett.*, 24:243–248, 1974. 4
- Falorsi, L., de Haan, P., Davidson, T. R., De Cao, N., Weiler, M., Forré, P., and Cohen, T. S. Explorations in homeomorphic variational auto-encoding. *arXiv preprint arXiv:1807.04689*, 2018. 1
- Falorsi, L., de Haan, P., Davidson, T. R., and Forré, P. Reparameterizing distributions on lie groups. *arXiv preprint arXiv:1903.02958*, 2019. 1
- Frenkel, D. and Smit, B. *Understanding molecular simulation*. Academic Press, 2001. 1
- Germain, M., Gregor, K., Murray, I., and Larochelle, H. Made: Masked autoencoder for distribution estimation. In *International Conference on Machine Learning*, pp. 881–889, 2015. 1
- Grathwohl, W., Chen, R. T., Bettencourt, J., Sutskever, I., and Duvenaud, D. Ffjord: Free-form continuous dynamics for scalable reversible generative models. *arXiv preprint arXiv:1810.01367*, 2018. 1
- Hoffman, M., Sountsov, P., Dillon, J. V., Langmore, I., Tran, D., and Vasudevan, S. Neutra-lizing bad geometry in hamiltonian monte carlo using neural transport. *arXiv preprint arXiv:1903.03704*, 2019. 1
- Hoffman, M. D. Learning deep latent gaussian models with markov chain monte carlo. *International Conference on Machine Learning*, pp. 1510–1519, 2017. 1
- Huang, C.-W., Krueger, D., Lacoste, A., and Courville, A. Neural autoregressive flows. *arXiv preprint arXiv:1804.00779*, 2018. 1
- Jia, J. and Benson, A. R. Neural jumpstochastic differential equations. *arXiv preprint arXiv:1905.10403*, 2019. 1
- Kingma, D. P. and Ba, J. Adam: A method for stochastic optimization. *arXiv:1412.6980*, 2014. 6
- Kingma, D. P. and Dhariwal, P. Glow: Generative flow with invertible 1x1 convolutions. In *Advances in Neural Information Processing Systems*, pp. 10215–10224, 2018. 1
- Köhler, J., Klein, L., and Noé, F. Equivariant flows: sampling configurations for multi-body systems with symmetric energies. *arXiv preprint arXiv:1910.00753*, 2019. 1

- LeCun, Y., Bottou, L., Bengio, Y., and Haffner, P. Gradient-based learning applied to document recognition. *Proc. IEEE*, 86:2278–2324, 1998. 5
- Levy, D., Hoffman, M. D., and Sohl-Dickstein, J. Generalizing hamiltonian monte carlo with neural networks. *arXiv preprint arXiv:1711.09268*, 2017. 1
- Li, S.-H. and Wang, L. Neural network renormalization group. *Phys. Rev. Lett.*, 121:260601, 2018. 1, 2, 2, 3
- Li, X., Wong, T.-K. L., Chen, R. T. Q., and Duvenaud, D. Scalable gradients for stochastic differential equations. *arXiv preprint arXiv:2001.01328*, 2020. 1
- Liu, X., Si, S., Cao, Q., Kumar, S., and Hsieh, C.-J. Neural sde: Stabilizing neural ode networks with stochastic noise. *arXiv preprint arXiv:1906.02355*, 2019. 1
- Louizos, C. and Welling, M. Multiplicative normalizing flows for variational bayesian neural networks. In *Proceedings of the 34th International Conference on Machine Learning-Volume 70*, pp. 2218–2227. JMLR. org, 2017. 1
- Müller, T., McWilliams, B., Rousselle, F., Gross, M., and Novák, J. Neural importance sampling. *arXiv preprint arXiv:1808.03856*, 2018. 1, 1
- Neal, R. M. Annealed importance sampling. *arXiv preprint arXiv:physics/9803008*, 1998. 4
- Nicoli, K. A., Nakajima, S., Strodthoff, N., Samek, W., Müller, K.-R., and Kessel, P. Asymptotically unbiased estimation of physical observables with neural samplers. *arXiv:1910.13496*, 2019. 1, 2, 2
- Nilmeier, J. P., Crooks, G. E., Minh, D. D. L., and Chodera, J. D. Nonequilibrium candidate Monte Carlo is an efficient tool for equilibrium simulation. *Proc. Natl. Acad. Sci. USA*, 108:E1009–E1018, 2011. 1, 3, 4, 6, 6, 6
- Noé, F., Olsson, S., Köhler, J., and Wu, H. Boltzmann generators: Sampling equilibrium states of many-body systems with deep learning. *Science*, 365(6457):eaaw1147, 2019. 1, 2, 1, 3, 3, 5, 6
- Oord, A. v. d., Li, Y., Babuschkin, I., Simonyan, K., Vinyals, O., Kavukcuoglu, K., Driessche, G. v. d., Lockhart, E., Cobo, L. C., Stimberg, F., et al. Parallel wavenet: Fast high-fidelity speech synthesis. *arXiv preprint arXiv:1711.10433*, 2017. 1
- Papamakarios, G., Pavlakou, T., and Murray, I. Masked autoregressive flow for density estimation. In *Advances in Neural Information Processing Systems*, pp. 2338–2347, 2017. 1
- Papamakarios, G., Nalisnick, E., Rezende, D. J., Mohamed, S., and Lakshminarayanan, B. Normalizing flows for probabilistic modeling and inference. *arXiv preprint arXiv:1912.02762*, 2019. 1, 4
- Pearlman, D. A., Case, D. A., Caldwell, J. W., Ross, W. R., Iii, C. T. E., Debolt, S., Ferguson, D., Seibel, G., and Kollman, P. AMBER, a computer program for applying molecular mechanics, normal mode analysis, molecular dynamics and free energy calculations to elucidate the structures and energies of molecules. *Comp. Phys. Commun.*, 91:1–41, 1995. 6
- Rezende, D. J. and Mohamed, S. Variational inference with normalizing flows. *arXiv preprint arXiv:1505.05770*, 2015. 1, 5, 6, 6
- Salimans, T., Kingma, D., and Welling, M. Markov chain monte carlo and variational inference: Bridging the gap. In *International Conference on Machine Learning*, pp. 1218–1226, 2015. 1
- Sohl-Dickstein, J., Weiss, E. A., Maheswaranathan, N., and Ganguli, S. Deep unsupervised learning using nonequilibrium thermodynamics. *arXiv preprint arXiv:1503.03585*, 2015. 1
- Song, J., Zhao, S., and Ermon, S. A-nice-mc: Adversarial training for mcmc. In *Advances in Neural Information Processing Systems*, pp. 5140–5150, 2017. 1
- Tabak, E. G. and Turner, C. V. A family of nonparametric density estimation algorithms. *Communications on Pure and Applied Mathematics*, 66(2):145–164, 2013. 1
- Tabak, E. G., Vanden-Eijnden, E., et al. Density estimation by dual ascent of the log-likelihood. *Communications in Mathematical Sciences*, 8(1):217–233, 2010. 1
- Tomczak, J. M. and Welling, M. Improving variational auto-encoders using householder flow. *arXiv preprint arXiv:1611.09630*, 2016. 1
- Toth, P., Rezende, D. J., Jaegle, A., Racanière, S., Botev, A., and Higgins, I. Hamiltonian generative networks. *arXiv preprint arXiv:1909.13789*, 2019. 5
- Tzen, B. and Raginsky, M. Neural stochastic differential equations: Deep latent gaussian models in the diffusion limit. *arXiv preprint arXiv:1905.09883*, 2019. 1
- Xiao, H., Rasul, K., and Vollgraf, R. Fashion-mnist: a novel image dataset for benchmarking machine learning algorithms. *arXiv preprint arXiv:cs.LG/1708.07747*, 2017. 5
- Zhang, L., Wang, L., et al. Monge-ampere flow for generative modeling. *arXiv preprint arXiv:1809.10188*, 2018. 1

Supplementary Material

Proof of SNV importance weights (Eq. 21)

Considering

$$\begin{aligned}
 \mathbb{E}_{\mu_X}[O] &= \int \mu_X(\mathbf{x})O(\mathbf{x})d\mathbf{x} \\
 &= \iint \mu_X(\mathbf{x})\mathbb{P}_b(\mathbf{x} \rightarrow \mathbf{z})O(\mathbf{x})d\mathbf{z}d\mathbf{x} \\
 &= \iint \mu_Z(\mathbf{z})\mathbb{P}_f(\mathbf{z} \rightarrow \mathbf{x}) \\
 &\quad \cdot \left[\frac{\mu_X(\mathbf{x})\mathbb{P}_b(\mathbf{x} \rightarrow \mathbf{z})}{\mu_Z(\mathbf{z})\mathbb{P}_f(\mathbf{z} \rightarrow \mathbf{x})} O(\mathbf{x}) \right] d\mathbf{z}d\mathbf{x} \\
 &= \mathbb{E}_f \left[\frac{\mu_X(\mathbf{x})\mathbb{P}_b(\mathbf{x} \rightarrow \mathbf{z})}{\mu_Z(\mathbf{z})\mathbb{P}_f(\mathbf{z} \rightarrow \mathbf{x})} O(\mathbf{x}) \right]
 \end{aligned}$$

In practice, we do not know the normalization constant of μ_X and we therefore replace $\frac{\mu_X(\mathbf{x})\mathbb{P}_b(\mathbf{x} \rightarrow \mathbf{z})}{\mu_Z(\mathbf{z})\mathbb{P}_f(\mathbf{z} \rightarrow \mathbf{x})}$ by the unnormalized path weights in Eq. (19). Then we must then normalize the estimator for expectation values, obtaining:

$$\frac{\sum_{k=1}^N \mathbf{w}(\mathbf{z}_k \rightarrow \mathbf{x}_k)O(\mathbf{x}_k)}{\sum_{k=1}^N \mathbf{w}(\mathbf{z}_k \rightarrow \mathbf{x}_k)} \xrightarrow{p} \mathbb{E}_\mu[O]$$

which converges towards $\mathbb{E}_\mu[O]$ with $N \rightarrow \infty$ according to the law of large numbers.

Derivation of the deterministic layer probability ratio

In order to work with delta distributions, we define $\delta^\sigma(\mathbf{x}) = \mathcal{N}(\mathbf{x}; \mathbf{0}, \sigma\mathbf{I})$, i.e. a Gaussian normal distribution with mean $\mathbf{0}$ and variance σ and then consider the limit $\sigma \rightarrow 0^+$. In the case where $\sigma > 0$, by defining

$$q_t^\sigma(\mathbf{y}_t \rightarrow \mathbf{y}_{t+1}) = \delta^\sigma(\mathbf{y}_{t+1} - F_t(\mathbf{y}_t)),$$

and

$$\begin{aligned}
 \tilde{q}_t^\sigma(\mathbf{y}_{t+1} \rightarrow \mathbf{y}_t) &= \frac{p_t(\mathbf{y}_t)q_t^\sigma(\mathbf{y}_t \rightarrow \mathbf{y}_{t+1})}{\int p_t(\mathbf{y})q_t^\sigma(\mathbf{y} \rightarrow \mathbf{y}_{t+1})d\mathbf{y}} \\
 &= \frac{p_t(\mathbf{y}_t)\delta^\sigma(\mathbf{y}_{t+1} - F_t(\mathbf{y}_t))}{\int p_t(\mathbf{y})\delta^\sigma(\mathbf{y}_{t+1} - F_t(\mathbf{y}))d\mathbf{y}},
 \end{aligned}$$

we have

$$\frac{\tilde{q}_t^\sigma(\mathbf{y}_{t+1} \rightarrow \mathbf{y}_t)}{q_t^\sigma(\mathbf{y}_t \rightarrow \mathbf{y}_{t+1})} = \frac{p_t(\mathbf{y}_t)}{\int p_t(\mathbf{y})\delta^\sigma(\mathbf{y}_{t+1} - F_t(\mathbf{y}))d\mathbf{y}},$$

where $p_t(\mathbf{y}_t)$ denotes the marginal distribution of \mathbf{y}_t . By considering

$$\begin{aligned}
 &\lim_{\sigma \rightarrow 0^+} \int p_t(\mathbf{y})\delta^\sigma(\mathbf{y}_{t+1} - F_t(\mathbf{y}))d\mathbf{y} \\
 &= \lim_{\sigma \rightarrow 0^+} \int p_t(F_t^{-1}(\mathbf{y}'))\delta^\sigma(\mathbf{y}_{t+1} - \mathbf{y}') \left| \det \left(\frac{\partial F_t^{-1}(\mathbf{y}')}{\partial \mathbf{y}'} \right) \right| d\mathbf{y}' \\
 &= p_t(F_t^{-1}(\mathbf{y}_{t+1})) \left| \det \left(\frac{\partial F_t^{-1}(\mathbf{y}_{t+1})}{\partial \mathbf{y}_{t+1}} \right) \right| \\
 &= p_t(\mathbf{y}_t) |\det \mathbf{J}_t(\mathbf{y}_t)|^{-1}
 \end{aligned}$$

and using the definition of ΔS_t in terms of path probability ratios, we obtain:

$$\begin{aligned}
 e^{\Delta S_t} &= \frac{\tilde{q}_t(\mathbf{y}_{t+1} \rightarrow \mathbf{y}_t)}{q_t(\mathbf{y}_t \rightarrow \mathbf{y}_{t+1})} = \lim_{\sigma \rightarrow 0^+} \frac{\tilde{q}_t^\sigma(\mathbf{y}_{t+1} \rightarrow \mathbf{y}_t)}{q_t^\sigma(\mathbf{y}_t \rightarrow \mathbf{y}_{t+1})} \\
 &= \lim_{\sigma \rightarrow 0^+} \frac{p_t(\mathbf{y}_t)}{\int p_t(\mathbf{y})\delta^\sigma(\mathbf{y}_{t+1} - F_t(\mathbf{y}))d\mathbf{y}} \\
 &= |\det \mathbf{J}_t(\mathbf{y}_t)|
 \end{aligned}$$

and thus

$$\Delta S_t = \log |\det \mathbf{J}_t(\mathbf{y}_t)|$$

Derivation of the overdamped Langevin path probability ratio

These results follow (Nilmeier et al., 2011). The backward step is realized by

$$\mathbf{y}_t = \mathbf{y}_{t+1} - \epsilon_t \nabla u_\lambda(\mathbf{y}_{t+1}) + \sqrt{\frac{2\epsilon_t}{\beta}} \tilde{\boldsymbol{\eta}}_t. \quad (23)$$

Combining Equations (22) and (23):

$$-\epsilon_t \nabla u_\lambda(\mathbf{y}_t) + \sqrt{\frac{2\epsilon_t}{\beta}} \boldsymbol{\eta}_t = \epsilon_t \nabla u_\lambda(\mathbf{y}_{t+1}) - \sqrt{\frac{2\epsilon_t}{\beta}} \tilde{\boldsymbol{\eta}}_t.$$

and thus

$$\tilde{\boldsymbol{\eta}}_t = \sqrt{\frac{\epsilon_t \beta}{2}} [\nabla u_\lambda(\mathbf{y}_t) + \nabla u_\lambda(\mathbf{y}_{t+1})] - \boldsymbol{\eta}_t$$

Resulting in the path probability ratio:

$$\begin{aligned}
 e^{\Delta S_t} &= \frac{q_t(\mathbf{y}_{t+1} \rightarrow \mathbf{y}_t)}{q_t(\mathbf{y}_t \rightarrow \mathbf{y}_{t+1})} = \frac{p(\tilde{\boldsymbol{\eta}}_t) \left| \frac{\partial \mathbf{y}_t}{\partial \tilde{\boldsymbol{\eta}}_t} \right|}{p(\boldsymbol{\eta}_t) \left| \frac{\partial \mathbf{y}_{t+1}}{\partial \boldsymbol{\eta}_t} \right|} \\
 &= \frac{p(\tilde{\boldsymbol{\eta}}_t)}{p(\boldsymbol{\eta}_t)} = e^{-\frac{1}{2}(\|\tilde{\boldsymbol{\eta}}_t\|^2 - \|\boldsymbol{\eta}_t\|^2)}.
 \end{aligned}$$

and thus

$$-\Delta S_t = \frac{1}{2} (\|\tilde{\boldsymbol{\eta}}_t\|^2 - \|\boldsymbol{\eta}_t\|^2)$$

Derivation of the Langevin probability ratio

These results follow (Nilmeier et al., 2011). We define constants:

$$\begin{aligned} c_1 &= \frac{\Delta t}{2m} \\ c_2 &= \sqrt{\frac{4\gamma m}{\Delta t \beta}} \\ c_3 &= 1 + \frac{\gamma \Delta t}{2} \end{aligned}$$

Then, the forward step of Brooks-Brünger-Karplus (BBK, leap-frog) Langevin dynamics is defined as:

$$\mathbf{v}' = \mathbf{v}_t + c_1 [-\nabla u_\lambda(\mathbf{x}_t) - \gamma m \mathbf{v}_t + c_2 \boldsymbol{\eta}_t] \quad (24)$$

$$\mathbf{x}_{t+1} = \mathbf{x}_t + \Delta t \mathbf{v}' \quad (25)$$

$$\mathbf{v}_{t+1} = \frac{1}{c_3} [\mathbf{v}' + c_1 (-\nabla u_\lambda(\mathbf{x}_{t+1}) + c_2 \boldsymbol{\eta}'_t)] \quad (26)$$

Note that the factor 4 in sqrt is different from (Nilmeier et al., 2011) – this factor is needed as we employ $\Delta t/2$ in both half-steps. The backward step with reversed momenta, $(\mathbf{x}_{t+1}, -\mathbf{v}_{t+1}) \rightarrow (\mathbf{x}_t, -\mathbf{v}_t)$ is then defined by:

$$\mathbf{v}'' = -\mathbf{v}_{t+1} + c_1 [-\nabla u_\lambda(\mathbf{x}_{t+1}) + \gamma m \mathbf{v}_{t+1} + c_2 \tilde{\boldsymbol{\eta}}_t] \quad (27)$$

$$\mathbf{x}_t = \mathbf{x}_{t+1} + \Delta t \mathbf{v}'' \quad (28)$$

$$-\mathbf{v}_t = \frac{1}{c_3} [\mathbf{v}'' + c_1 (-\nabla u_\lambda(\mathbf{x}_t) + c_2 \tilde{\boldsymbol{\eta}}'_t)] \quad (29)$$

To compute the momenta $\tilde{\boldsymbol{\eta}}_t, \tilde{\boldsymbol{\eta}}'_t$ that realize the reverse step, we first combine Eqs. (25-28) to obtain:

$$\mathbf{v}' = -\mathbf{v}'' \quad (30)$$

Combining Eqs. (26), (27) and (30), we obtain:

$$\left(1 + \frac{\gamma \Delta t}{2}\right) \mathbf{v}_{t+1} = \mathbf{v}' + c_1 (-\nabla u_\lambda(\mathbf{x}_{t+1}) + c_2 \boldsymbol{\eta}'_t)$$

$$\left(1 - \frac{\gamma \Delta t}{2}\right) \mathbf{v}_{t+1} = \mathbf{v}' + c_1 (-\nabla u_\lambda(\mathbf{x}_{t+1}) + c_2 \tilde{\boldsymbol{\eta}}_t),$$

and:

$$\tilde{\boldsymbol{\eta}}_t = \boldsymbol{\eta}'_t - \sqrt{\gamma \Delta t m \beta} \mathbf{v}_{t+1}$$

Combining Eqs. (24), (29) and (30), we obtain:

$$-\mathbf{v}_t \left(1 - \frac{\gamma \Delta t}{2}\right) = \mathbf{v}'' + c_1 (-\nabla u_\lambda(\mathbf{x}_t) + c_2 \boldsymbol{\eta}_t)$$

$$-\mathbf{v}_t \left(1 + \frac{\gamma \Delta t}{2}\right) = \mathbf{v}'' + c_1 (-\nabla u_\lambda(\mathbf{x}_t) + c_2 \tilde{\boldsymbol{\eta}}'_t),$$

and:

$$-\mathbf{v}_t \left(1 - \frac{\gamma \Delta t}{2}\right) - c_2 \boldsymbol{\eta}_t = -\mathbf{v}_t \left(1 + \frac{\gamma \Delta t}{2}\right) - c_2 \tilde{\boldsymbol{\eta}}'_t$$

$$\tilde{\boldsymbol{\eta}}'_t = \boldsymbol{\eta}_t - \sqrt{\gamma \Delta t m \beta} \mathbf{v}_t$$

To compute the path probability ratio we introduce the Jacobian

$$J(\boldsymbol{\eta}_t, \boldsymbol{\eta}'_t) = \det \begin{bmatrix} \frac{\partial \mathbf{x}_{t+1}}{\partial \boldsymbol{\eta}_t} & \frac{\partial \mathbf{v}_{t+1}}{\partial \boldsymbol{\eta}_t} \\ \frac{\partial \mathbf{x}_{t+1}}{\partial \boldsymbol{\eta}'_t} & \frac{\partial \mathbf{v}_{t+1}}{\partial \boldsymbol{\eta}'_t} \end{bmatrix}$$

and find:

$$\begin{aligned} e^{\Delta S_t} &= \frac{\tilde{q}_t((\mathbf{x}_{t+1}, -\mathbf{v}_{t+1}) \rightarrow (\mathbf{x}_t, \mathbf{v}_t))}{q_t((\mathbf{x}_t, \mathbf{v}_t) \rightarrow (\mathbf{x}_{t+1}, -\mathbf{v}_{t+1}))} \\ &= \frac{p(\tilde{\boldsymbol{\eta}}_t) p(\tilde{\boldsymbol{\eta}}'_t) J(\tilde{\boldsymbol{\eta}}_t, \tilde{\boldsymbol{\eta}}'_t)}{p(\boldsymbol{\eta}_t) p(\boldsymbol{\eta}'_t) J(\boldsymbol{\eta}_t, \boldsymbol{\eta}'_t)} \\ -\Delta S_t &= \frac{1}{2} \left((\|\tilde{\boldsymbol{\eta}}_t\|^2 + \|\tilde{\boldsymbol{\eta}}'_t\|^2) - (\|\boldsymbol{\eta}_t\|^2 + \|\boldsymbol{\eta}'_t\|^2) \right) \end{aligned}$$

where the Jacobian ratio cancels as the Jacobians are independent of the noise variables.

Markov Chain Monte Carlo

We propose a new state according to the proposal density

$$\mathbf{y}^* \sim g_t(\mathbf{y}^* | \mathbf{y}_t)$$

and accept this state with probability

$$p_{\text{acc}}(\mathbf{y}_t \rightarrow \mathbf{y}^*) = \min \left\{ 1, e^{-(u_\lambda(\mathbf{y}^*) - u_\lambda(\mathbf{y}_t))} \frac{g_t(\mathbf{y}_t | \mathbf{y}^*)}{g_t(\mathbf{y}^* | \mathbf{y}_t)} \right\}.$$

Then we have, if we accept:

$$\begin{aligned} q_t(\mathbf{y}_t \rightarrow \mathbf{y}^* \rightarrow \text{acc} \rightarrow \mathbf{y}_{t+1} = \mathbf{y}^*) \\ &= g_t(\mathbf{y}_{t+1} | \mathbf{y}_t) p_{\text{acc}}(\mathbf{y}_t \rightarrow \mathbf{y}_{t+1}) \\ q_t(\mathbf{y}_{t+1} \rightarrow \mathbf{y}^* \rightarrow \text{acc} \rightarrow \mathbf{y}_t = \mathbf{y}^*) \\ &= g_t(\mathbf{y}_t | \mathbf{y}_{t+1}) p_{\text{acc}}(\mathbf{y}_{t+1} \rightarrow \mathbf{y}_t) \end{aligned}$$

and if we reject:

$$\begin{aligned} q_t(\mathbf{y}_t \rightarrow \mathbf{y}^* \rightarrow \text{rej} \rightarrow \mathbf{y}_{t+1} = \mathbf{y}_t) \\ &= g_t(\mathbf{y}^* | \mathbf{y}_t) (1 - p_{\text{acc}}(\mathbf{y}_t \rightarrow \mathbf{y}^*)) \\ q_t(\mathbf{y}_{t+1} = \mathbf{y}_t \rightarrow \mathbf{y}^* \rightarrow \text{rej} \rightarrow \mathbf{y}_t) \\ &= g_t(\mathbf{y}^* | \mathbf{y}_t) (1 - p_{\text{acc}}(\mathbf{y}_t \rightarrow \mathbf{y}^*)) \end{aligned}$$

Then we have the path probability ratio:

$$\frac{q_t(\mathbf{y}_{t+1} \rightarrow \cdots \rightarrow \mathbf{y}_t)}{q_t(\mathbf{y}_t \rightarrow \cdots \rightarrow \mathbf{y}_{t+1})} = \begin{cases} \frac{g_t(\mathbf{y}_t | \mathbf{y}_{t+1}) p_{\text{acc}}(\mathbf{y}_{t+1} \rightarrow \mathbf{y}_t)}{g_t(\mathbf{y}_{t+1} | \mathbf{y}_t) p_{\text{acc}}(\mathbf{y}_t \rightarrow \mathbf{y}_{t+1})} & \text{accept} \\ 1 & \text{reject} \end{cases}$$

with

$$\frac{p_{\text{acc}}(\mathbf{y}_{t+1} \rightarrow \mathbf{y}_t)}{p_{\text{acc}}(\mathbf{y}_t \rightarrow \mathbf{y}_{t+1})} = \frac{\min \left\{ 1, e^{-(u(\mathbf{y}_t) - u(\mathbf{y}_{t+1}))} \frac{g_t(\mathbf{y}_{t+1} | \mathbf{y}_t)}{g_t(\mathbf{y}_t | \mathbf{y}_{t+1})} \right\}}{\min \left\{ 1, e^{-(u(\mathbf{y}_{t+1}) - u(\mathbf{y}_t))} \frac{g_t(\mathbf{y}_t | \mathbf{y}_{t+1})}{g_t(\mathbf{y}_{t+1} | \mathbf{y}_t)} \right\}}.$$

if $e^{-(u_\lambda(\mathbf{y}_t) - u_\lambda(\mathbf{y}_{t+1})) \frac{g_t(\mathbf{y}_{t+1} | \mathbf{y}_t)}{g_t(\mathbf{y}_t | \mathbf{y}_{t+1})}} \geq 1$:

$$\frac{p_{\text{acc}}(\mathbf{y}_{t+1} \rightarrow \mathbf{y}_t)}{p_{\text{acc}}(\mathbf{y}_t \rightarrow \mathbf{y}_{t+1})} = \frac{g_t(\mathbf{y}_{t+1} | \mathbf{y}_t)}{g_t(\mathbf{y}_t | \mathbf{y}_{t+1})} e^{-(u_\lambda(\mathbf{y}_t) - u_\lambda(\mathbf{y}_{t+1}))}$$

Otherwise the same:

$$\frac{p_{\text{acc}}(\mathbf{y}_{t+1} \rightarrow \mathbf{y}_t)}{p_{\text{acc}}(\mathbf{y}_t \rightarrow \mathbf{y}_{t+1})} = \frac{g_t(\mathbf{y}_{t+1} | \mathbf{y}_t)}{g_t(\mathbf{y}_t | \mathbf{y}_{t+1})} e^{-(u_\lambda(\mathbf{y}_t) - u_\lambda(\mathbf{y}_{t+1}))}$$

So the path probability is equal to:

$$\begin{aligned} & \frac{q_t(\mathbf{y}_{t+1} \rightarrow \dots \rightarrow \mathbf{y}_t)}{q_t(\mathbf{y}_t \rightarrow \dots \rightarrow \mathbf{y}_{t+1})} \\ &= \begin{cases} \frac{g_t(\mathbf{y}_t | \mathbf{y}_{t+1})}{g_t(\mathbf{y}_{t+1} | \mathbf{y}_t)} e^{u_\lambda(\mathbf{y}_{t+1}) - u_\lambda(\mathbf{y}_t)} & \text{accept} \\ 1 & \text{reject} \end{cases} \end{aligned}$$

Thus we have

$$\Delta S_t = \begin{cases} u_\lambda(\mathbf{y}_{t+1}) - u_\lambda(\mathbf{y}_t) + \log \frac{g_t(\mathbf{y}_t | \mathbf{y}_{t+1})}{g_t(\mathbf{y}_{t+1} | \mathbf{y}_t)} & \text{accept} \\ 0 & \text{reject} \end{cases}$$

For symmetric proposals, this is always:

$$\Delta S_t = u_\lambda(\mathbf{y}_{t+1}) - u_\lambda(\mathbf{y}_t)$$

Details on using SNFs for variational inference

In the last results section we use SNFs in the latent space of a variational autoencoder (VAE). For a given data set $\{\mathbf{s}_1, \dots, \mathbf{s}_N\}$, the decoder D of VAE characterizes each \mathbf{s} as a random variable with a tractable distribution $\mathbb{P}_D(\mathbf{s} | \mathbf{x})$ depending on a unknown latent variable \mathbf{x} , and the prior distribution is also assumed to be a tractable one (e.g., the normal distribution). Then D defines a joint distribution of (\mathbf{x}, \mathbf{s}) in the form of

$$\mathbb{P}_D(\mathbf{x}, \mathbf{s}) = \mathcal{N}(\mathbf{x} | \mathbf{0}, \mathbf{I}) \cdot \mathbb{P}_D(\mathbf{s} | \mathbf{x}).$$

For a given \mathbf{s} , we can utilize the SNF to approximate the posterior distribution

$$\mathbb{P}_D(\mathbf{x} | \mathbf{s}) = \frac{\mathbb{P}_D(\mathbf{x}, \mathbf{s})}{\mathbb{P}_D(\mathbf{s})}.$$

For convenience of notation, we define $\mu_X(\mathbf{x}) = \mathbb{P}_D(\mathbf{x} | \mathbf{s})$ and $u_X(\mathbf{x}) = -\log \mathbb{P}_D(\mathbf{x}, \mathbf{s})$. Then parameters of SNF can be trained by minimizing the variational bound J_{KL} of the KL divergence, and it provides a variational upper bound of the negative log-likelihood of \mathbf{s} as follows:

$$\begin{aligned} J_{KL} &= \mathbb{E}_{\mathbf{z} \sim \mu_{\mathbf{Z}}, \mathbf{y}_1, \dots, \mathbf{y}_T} [u_X(\mathbf{y}_T) - \sum_{t=0}^{T-1} \Delta S_t] \\ &= \mathbb{E}_{\mathbf{z} \sim \mu_{\mathbf{Z}}, \mathbf{y}_1, \dots, \mathbf{y}_T} [-\log \mu_X(\mathbf{y}_T) - \sum_{t=0}^{T-1} \Delta S_t] \\ &\quad - \log \mathbb{P}_D(\mathbf{s}) \\ &= \text{KL}(\mu_{\mathbf{Z}}(\mathbf{z}) \mathbb{P}_f(\mathbf{z} \rightarrow \mathbf{x}) \parallel \mu_X(\mathbf{x}) \mathbb{P}_b(\mathbf{x} \rightarrow \mathbf{z})) \\ &\quad - \log \mathbb{P}_D(\mathbf{s}) \\ &\geq -\log \mathbb{P}_D(\mathbf{s}) \end{aligned}$$

If the SNF only contains deterministic transformations, the J_{KL} is equivalent to the $\mathcal{F}(x)$ in (Rezende & Mohamed, 2015). In our numerical experiments, $J_{KL}(\mathbf{s})$ is estimated as

$$\hat{J}_{KL}(\mathbf{s}) = \frac{1}{M} \sum_{i=1}^M u_X(\mathbf{y}_T^{(i)}) - \sum_{t=0}^{T-1} \Delta S_t^{(i)} \quad (31)$$

by sampling M paths $\{(\mathbf{y}_0^{(i)}, \dots, \mathbf{y}_T^{(i)})\}_{i=1}^M$ for each \mathbf{s} and $M = 5$. All the parameters of D and SNF are trained to minimize the mean value of $\hat{J}_{KL}(\mathbf{s})$ over all \mathbf{s} . After getting a decoder D , we approximate $-\log \mathbb{P}_D(\mathbf{s})$ as follows:

1. Train a RNVP F_{LL} by minimizing the mean value of

$$\begin{aligned} & \log q_{LL}(F_{LL}(\mathbf{z}; \mathbf{s}) | \mathbf{s}) \\ & \quad - \log \mathcal{N}(F_{LL}(\mathbf{z}; \mathbf{s}) | \mathbf{0}, \mathbf{I}) - \log \mathbb{P}_D(\mathbf{s} | F_{LL}(\mathbf{z}; \mathbf{s})) \end{aligned}$$

over all \mathbf{s} in the training data set and $\mathbf{z} \sim \mathcal{N}(\mathbf{z} | \mathbf{0}, \mathbf{I})$, where $F_{LL}(\mathbf{z}; \mathbf{s})$ is an invertible function with respect to \mathbf{z} for a given \mathbf{s} , and

$$\begin{aligned} & \log q_{LL}(\mathbf{x} | \mathbf{s}) \\ &= \log \mathcal{N}(\mathbf{z} | \mathbf{0}, \mathbf{I}) - \log \left| \det \left(\frac{\partial \mathbf{x}}{\partial \mathbf{z}} \right) \right| \end{aligned}$$

denotes the probability density of the random variable $\mathbf{x} = F_{LL}(\mathbf{z}; \mathbf{s})$. Notice that the model defined by the above equation can be interpreted as a one-step SNF with only one deterministic step $\mathbf{x} = F_{LL}(\mathbf{z}; \mathbf{s})$ for a fixed \mathbf{s} .

2. Considering

$$\begin{aligned} & \mathbb{P}_D(\mathbf{s}) \\ &= \int \mathcal{N}(\mathbf{x} | \mathbf{0}, \mathbf{I}) \mathbb{P}_D(\mathbf{s} | \mathbf{x}) d\mathbf{x} \\ &= \int q_{LL}(\mathbf{x} | \mathbf{s}) \frac{\mathcal{N}(\mathbf{x} | \mathbf{0}, \mathbf{I}) \mathbb{P}_D(\mathbf{s} | \mathbf{x})}{q_{LL}(\mathbf{x} | \mathbf{s})} d\mathbf{x} \\ &= \mathbb{E}_{\mathbf{x} \sim q_{LL}(\mathbf{x} | \mathbf{s})} \left[\frac{\mathcal{N}(\mathbf{x} | \mathbf{0}, \mathbf{I}) \mathbb{P}_D(\mathbf{s} | \mathbf{x})}{q_{LL}(\mathbf{x} | \mathbf{s})} \right] \\ &= \mathbb{E}_{\mathbf{z} \sim \mathcal{N}(\mathbf{z} | \mathbf{0}, \mathbf{I})} \left[\frac{\mathcal{N}(F_{LL}(\mathbf{z}; \mathbf{s}) | \mathbf{0}, \mathbf{I}) \mathbb{P}_D(\mathbf{s} | F_{LL}(\mathbf{z}; \mathbf{s}))}{\mathcal{N}(\mathbf{z} | \mathbf{0}, \mathbf{I}) \left| \det \left(\frac{\partial F_{LL}(\mathbf{z}; \mathbf{s})}{\partial \mathbf{z}} \right) \right|^{-1}} \right], \end{aligned}$$

we can draw N samples $\mathbf{z}^{(1)}, \dots, \mathbf{z}^{(N)}$ and approximate $\mathbb{P}_D(\mathbf{s})$ by

$$\hat{\mathbb{P}}_D(\mathbf{s}) = \frac{1}{N} \sum_{i=1}^N \frac{\mathcal{N}(F_{LL}(\mathbf{z}^{(i)}; \mathbf{s}) | \mathbf{0}, \mathbf{I}) \mathbb{P}_D(\mathbf{s} | F_{LL}(\mathbf{z}^{(i)}; \mathbf{s}))}{\mathcal{N}(\mathbf{z}^{(i)} | \mathbf{0}, \mathbf{I}) \left| \det \left(\frac{\partial F_{LL}(\mathbf{z}^{(i)}; \mathbf{s})}{\partial \mathbf{z}} \right) \right|^{-1}}.$$

In experiments, N is set to be 2000.

In table 1, the first column is the mean value of $\hat{J}_{KL}(\mathbf{s})$ on the test data set as a variational bound of the mean of $-\log p(\mathbf{s})$ (related to Fig.4a in (Rezende & Mohamed, 2015)). The second column is the mean value of $-\log \hat{\mathbb{P}}_D(\mathbf{s})$ on the test data set (related to Fig.4c in (Rezende & Mohamed, 2015)).

Hyper-parameters and other benchmark details

All experiments were run using PyTorch 1.2 and on GTX1080Ti cards. Optimization uses Adam (Kingma & Ba, 2014) with step-size 0.001 and otherwise default parameters. All deterministic flow transformations use RealNVP (Dinh et al., 2016). A RealNVP block is defined by two subsequent RealNVP layers that are swapped such that each channels gets transformed once as a function of the other channel. In the RealNVP scaling and translation transformer networks, fully connected ReLU networks were used.

Double well examples in Figures 1 and 5

- Both normalizing flow and SNF networks use 3 RealNVP blocks with 2 hidden layers and [64, 64] nodes in their transformers. The SNF additionally uses 20 Metropolis MC steps per block using a Gaussian proposal density with standard deviation 0.25.
- Training is done by minimizing J_{ML} for 300 iterations and $\frac{1}{2}J_{ML} + \frac{1}{2}KL$ for 300 iterations using a batch-size of 128.
- “Biased data” is defined by running local Metropolis MC in each of the two wells. These simulations do not transition to the other well and we use 1000 data points in each well for training.
- “Unbiased data” is produced by running Metropolis MC with a large proposal step (standard deviation 1.5) to convergence and retaining 10000 data points for training.

Two-dimensional image densities in Figures 3 and 4

- Standard normalizing flow (column 1) uses 5 RealNVP blocks with 3 hidden layers and [64, 64, 64] nodes in their transformers. Training was done by minimizing J_{ML} for 2000 iterations with batch-size 250.
- Purely stochastic flow (column 2) uses five blocks with 10 Metropolis MC steps each using a Gaussian proposal density with standard deviation 0.1.
- SNF (column 3) uses 5 blocks (RNVP block and 10 Metropolis MC steps with same parameters as above).

Training was done by minimizing J_{ML} for 6000 iterations with batch-size 250.

Alanine dipeptide in Fig. 6

- Normalizing flow uses 3 RealNVP blocks with 3 hidden layers and [128, 128, 128] nodes in their transformers. Training was done by minimizing J_{ML} for 1000 iterations with batch-size 256.
- SNF uses the same architecture and training parameters, but additionally 20 Metropolis MC steps each using a Gaussian proposal density with standard deviation 0.1.
- As a last flow layer before \mathbf{x} , we used an invertible transformation between Cartesian coordinates and internal coordinates (bond lengths, angles, torsion angles) following the procedure described in (Noé et al., 2019). The internal coordinates were normalized by removing the mean and dividing by the standard deviation of their values in the training data.
- Training data: We set up Alanine dipeptide in vacuum using OpenMMTools. Parameters are defined by the force field ff96 of the AMBER program (Pearlman et al., 1995). Simulations are run at standard OpenMMTools parameters with no bond constraints, 1 femtosecond time-step for 10^6 time-steps (1 nanosecond) at a temperature of 1000 K, which results in rapid exploration of the ϕ/ψ torsion angles and a few hundred transitions between metastable states. 10^5 atom positions were saved as training data.

MNIST and Fashion-MNIST VAE in Table 1

- The latent space dimension was set to 50. The decoder consists of 2 fully connected hidden layers, with 1024 units and ReLU non-linearities for each hidden layer. The activation function of the the output layer is sigmoid function. $\mathbb{P}_D(\mathbf{s}|\mathbf{x})$ is defined as

$$\begin{aligned} \log \mathbb{P}_D(\mathbf{s}|\mathbf{x}) &= \log \mathbb{P}_D(\mathbf{s}|D(\mathbf{x})) \\ &= \sum_{i=1}^{784} [s]_i \log[D(\mathbf{x})]_i + (1 - [s]_i) \log(1 - [D(\mathbf{x})]_i), \end{aligned}$$

where $[s]_i$, $[D(\mathbf{x})]_i$ denote the i th pixel of \mathbf{s} and the i th output of D .

- Adam algorithm is used to train all models. Training was done by minimizing \hat{J}_{KL} (see (31)) for 40 epochs with batch-size 128 and step size 10^{-3} unless otherwise stated.

- In simple VAE, the encoder E consists of 2 fully connected hidden layers, with 1024 nodes and ReLU nonlinearities for each hidden layer. The encoder has 100 outputs, where the activation function of the first 50 outputs is the linear function and the activation function of the last 50 outputs is the absolute value function. The transformation from \mathbf{z} to \mathbf{x} is given by

$$[\mathbf{x}]_i = [E(\mathbf{s})]_i + [\mathbf{z}]_i \cdot [E(\mathbf{s})]_{i+50}. \quad (32)$$

- MCMC uses 30 Metropolis MC steps each using a overdamped Langevin proposal, where the interpolated potential are used. The interpolation coefficients and the step size of the proposal are both trained as parameters of the flow.
- Normalizing flow uses 6 RealNVP blocks with 2 hidden layers and $[64, 64]$ nodes in their transformers.
- SNF uses three units with each unit consisting of 2 RealNVP blocks + 10 Metropolis MC steps, where architectures are the same as the above. During the training procedure, we first train parameters of the 6 RealNVP blocks without the Metropolis MC steps for 20 epochs, and then train all parameters for another 20 epochs. The training step size is 10^{-3} for the first 20 epochs and 10^{-4} for the last 20 epochs.
- For calculating the marginal likelihood $\mathbb{P}_D(\mathbf{s})$, F_{LL} uses 12 RealNVP blocks with 2 hidden layers and $[256, 256]$ nodes in their transformers.

Supplementary Figures

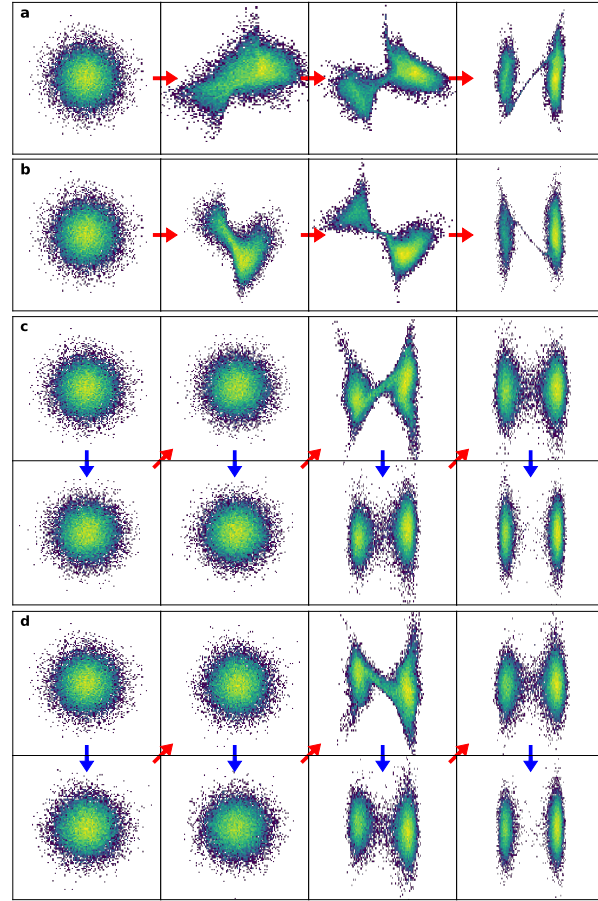


Figure 7. Reproducibility of normalizing flows for the double well. Red arrows indicate deterministic transformations (perturbations), blue arrows indicate stochastic dynamics (relaxations). **a-b)** Two independent runs of 3 RealNVP blocks (6 layers). **c-d)** Two independent runs of same architecture with 20 BD steps before/after RealNVP blocks.